ATLAS NOTE

ATL-PHYS-PUB-2014-003

March 17, 2014

Comparison of the response of the ATLAS detector to electromagnetic processes in data at 8 TeV and simulation using different GEANT 4 setups

The ATLAS Collaboration

ATL-PHYS-PUB-2014-003
17 March 2014

Abstract

The response of the ATLAS detector to electromagnetic processes is compared in data at 8 TeV using $Z \rightarrow e^{+}e^{-}$ events and isolated direct photon candidates, and in simulated samples using different GEANT 4 versions and physics list.

1 Motivation

The plots presented in this note compare the response of the ATLAS detector to electromagnetic processes in data at 8 TeV, and in simulated samples using different GEANT 4 versions and physics lists. $Z \to e^+e^-$ events and isolated direct photon candidates are used. We present three series of plots:

- Comparison of electromagnetic shower shapes as described in simulation by two different GEANT4 versions (Section 4.1);
- Comparison of the $Z \to e^+e^-$ lineshape in pp data at $\sqrt{s} = 8$ TeV and in simulated samples using two different GEANT4 versions (Section 4.2);
- Comparison of the relative fraction of converted photons in pp data at $\sqrt{s} = 8$ TeV and in simulation using two different GEANT4 conversion models (Section 4.3).

A brief description of the Monte Carlo (MC) samples used in the plots is provided in Section 2, while Section 3 gives a brief overview of the selection in of electrons and photons in data.

2 Simulation samples and setups

A detailed description of the ATLAS event generation and simulation infrastructure is provided in Ref. [1].

For this study, $Z \to e^+e^-$ Monte Carlo (MC) samples are obtained using POWHEG [2] interfaced to PYTHIA 8 [3] with AU2CT10 tuning [4]. When appropriate, these simulated events go through the same selections as the data, as described in Section 3, and are corrected for a number of known discrepancies between data and simulation, e.g. the different distributions of average number of interactions per bunch crossing in data and MC; slight discrepancies in the electron trigger, identification and reconstruction efficiencies; the distributions of the primary vertex z position; the line-shape of the Z boson, to emulate a running Z boson width from the fixed width used in POWHEG.

Direct photon MC samples are obtained using PYTHIA 8 with AU2CT10 tuning. As for the $Z \to e^+e^-$ samples, these simulated events also go through the same selections as the data, and are moreover corrected for a number of known discrepancies, namely the different distributions of average number of interactions per bunch crossing in data and MC, the distributions of the primary vertex z position, and the distribution of the shower shapes in the LAr Electromagnetic Calorimeter (EMC) used to define the quality of the photon candidates.

The ATLAS detector response is simulated using the GEANT4 program [5]. In order to study the impact of different detector simulation setups, $Z \to e^+e^-$ and direct photon MC samples are produced using alternative GEANT4 versions, and using different physics lists:

- $Z \to e^+e^-$ **samples**
  - GEANT4 v. 9.4, including a fix for the electron multiple scattering bug affecting Urban93 models [6];
  - GEANT4 v. 9.6, using Urban95 models [6].

  Both samples have been simulated either without pileup overlay, in order to allow for a more sensitive comparison between GEANT4 versions (Section 4.1), or with full pileup overlay, and are used to compare the detector response to electrons in data (Section 4.2).

- **Direct photon samples**
  - `GEANT4` v. 9.4, using `Conv93` photon conversion model [7];
  - `GEANT4` v. 9.4, using `Conv95` photon conversion model [7].

  Both samples have been simulated including the pileup overlay, in order to allow for a direct comparison of the detector response to photons with data (Section 4.3).

3 Data selections

This study uses pp collision data at $\sqrt{s} = 8$ TeV collected by the ATLAS detector [8] in 2012. All events are requested to pass the standard ATLAS data quality requirements. Events where the ATLAS LAr EMC or the ATLAS Hadronic Calorimeter response is affected by transient problems are rejected.

Electron candidate selections

When the comparison is restricted exclusively to $Z \to e^+e^-$ MC samples (Section 4.2), electrons and positrons from $Z \to e^+e^-$ events are simply selected by requesting they have $|\eta_e| < 2.47$[1] , and $E_{\mathrm{T}}^e > 20$ GeV.

When instead data is compared to MC (Section 4.2), $Z \to e^+e^-$ candidates are initially selected from events satisfying a trigger requirement with either one electron candidate with $E_{\mathrm{T}} > 24$ GeV passing the medium quality selection and being loosely isolated, or with one electron candidate with $E_{\mathrm{T}} > 60$ GeV passing the medium quality selection. This medium quality selection is based on rectangular cuts on tracking information and calorimetric shower shapes, following the procedure described in Ref. [9], with selections optimized for the pileup level expected in 2012 pp collisions. These events must then contain exactly two electron candidates in the detector central region ($|\eta_e| < 2.47$), both satisfying the calorimetric quality requirements, passing the medium quality selection, and having a reconstructed transverse momentum, defined from the calibrated electromagnetic cluster energy and the polar angle measured in the ATLAS Inner Tracking Detector ID, above 27 GeV. Events are finally retained if the two electron candidates have opposite charges and an invariant mass in the range $80 < m_{ee} < 100$ GeV. An additional selection on the z position of the reconstructed primary vertex, $|z| < 150$ mm is applied to improve the agreement between the the primary vertex z distribution in data and simulation. This selection retains about 6.25 million events in the pp data collected by ATLAS at $\sqrt{s} = 8$ TeV in 2012, corresponding to an integrated luminosity of about 20.3 fb^{-1}. The same selections are applied to the correponding MC samples.

Direct photon candidate selections

Direct photon candidates are initially selected in data from events satisfying at least one of several single-photon triggers, each requiring the presence of a photon candidate passing the loose selection, based on calorimetric shower shapes, and having transverse momentum larger then 40, 60, 80, 100 and 120 GeV respectively. During the 2012 data-taking, no pre-scale was applied to the 120 GeV threshold trigger, and the collected total integrated luminosity amounts to about 20.3 fb^{-1}; increasing pre-scale factors were applied to the lower E_{T} threshold single photons triggers, leading to smaller integrated luminosities. These events must then have at least one reconstructed primary vertex with at least two

[1] ATLAS uses a right-handed coordinate system with its origin at the nominal interaction point (IP) in the centre of the detector and the z-axis along the beam pipe. The x-axis points from the IP to the centre of the LHC ring, and the y-axis points upward. Cylindrical coordinates (r, ϕ) are used in the transverse plane, ϕ being the azimuthal angle around the beam pipe. The pseudorapidity is defined in terms of the polar angle θ as $\eta = -\ln\tan(\theta/2)$.

associated tracks. They must contain at least one photon candidate in the detector precision region ($|\eta_\gamma| < 1.37$, or $1.56 \leq |\eta_\gamma| < 2.37$), satisfying calorimetric quality requirements, passing the tight quality selection, and having a reconstructed transverse momentum $E_{\mathrm{T}} > 25$ GeV. The photon tight quality selection is based on rectangular cuts on calorimetric shower shapes, following the procedure described in Ref. [10], with selections optimized for the pileup level expected in 2012 pp collisions. The isolation energy $E_{\mathrm{T}}^{\mathrm{iso}}$ associated to each photon candidate must be smaller than 3 GeV. $E_{\mathrm{T}}^{\mathrm{iso}}$ is computed as the sum of the transverse energies of noise-suppressed clusters in a cone of radius $R = \sqrt{(\eta - \eta^\gamma)^2 + (\phi - \phi^\gamma)^2} = 0.4$ centered around the photon direction, corrected by subtracting both the mean value of the small leakage of the photon energy outside its cluster, evaluated as a function of the photon transverse energy, and the estimated contributions from the underlying event and pileup. This correction is computed on an event-by-event basis using the method suggested in Ref. [11, 12] and first implemented in Ref. [13]. The same selections are applied to the correponding MC samples.

4 Response comparison

4.1 Electromagnetic shower shapes

The response of the ATLAS LAr EMC to electron-induced electromagnetic showers in data and MC is evaluated by studying the behavior of different shower shapes, sensitive to the properties of the shower development in the detector. These shower shapes are computed as follows:

- **Variables using the second compartment of the EMC (Middle)**
  - *Middle η energy ratio*

$$R_\eta = \frac{E^{S2}_{3\times7}}{E^{S2}_{7\times7}} \tag{1}$$

    is the ratio between the sum $E^{S2}_{3\times7}$ of the energies of the EMC Middle cells contained in a 3×7 $\eta \times \phi$ rectangle (measured in cell units), and the sum $E^{S2}_{7\times7}$ of the cell energies in a 7×7 rectangle, both centered around the cluster seed.
  - *Middle ϕ energy ratio*

$$R_\phi = \frac{E^{S2}_{3\times3}}{E^{S2}_{3\times7}} \tag{2}$$

    is defined similarly to R_η.
  - *Middle lateral width*

$$w_{\eta_2} = \sqrt{\frac{\sum E_i \eta_i^2}{\sum E_i} - \left(\frac{\sum E_i \eta_i}{\sum E_i}\right)^2} \tag{3}$$

    measures the shower lateral width in the EMC Middle, using all cells in a window $\eta\times\phi$ = 3×5 measured in cell units.

- **Variables using the first compartment of the EMC (Front)**
  - *Front lateral width (3 strips)*

$$w_{s\,3} = \sqrt{\frac{\sum E_i (i - i_{\max})^2}{\sum E_i}} \tag{4}$$

measures the shower width in the EMC Front, using 2 strip cells around the maximal energy deposit. The index i is the strip identification number along the η direction, $i_{\max}$ identifies the strip cell with the greatest energy; E_i is the energy deposit in each strip cell.

– *Front lateral width (total)*
$w_{s\,\mathrm{tot}}$ measures the shower width in the EMC Front using all cells in a window $\Delta\eta \times \Delta\phi = 0.0625 \times 0.2$, corresponding to approximately 20 strip cells in η and 2 in ϕ, and is computed as $w_{s\,3}$.

– *Front maxima relative ratio*

$$E_{\mathrm{ratio}} = \frac{E^{S\,1}_{1^{\mathrm{st}}\,\max} - E^{S\,1}_{2^{\mathrm{nd}}\,\max}}{E^{S\,1}_{1^{\mathrm{st}}\,\max} + E^{S\,1}_{2^{\mathrm{nd}}\,\max}} \tag{5}$$

measured the relative difference between the energy of the strip cell with the greatest energy $E^{S\,1}_{1^{\mathrm{st}}\,\max}$ and the energy in the strip cell with second greatest energy $E^{S\,1}_{2^{\mathrm{nd}}\,\max}$.

Discrepancies in the description of these variables by the ATLAS MC were observed in the past (see for instance Ref. [9]), and partially mitigated by an update of the GEANT4 version (4.9.3) combined with a change of the ATLAS geometry description (see for instance Ref. [14]).

The following plots show the dependency of such variables on the GEANT4 simulation setup. Figures 1, 2, 3, 4, 5, 6, show the R_η, R_ϕ, w_{η_2}, $w_{s\,3}$, $w_{s\,\mathrm{tot}}$ and E_{ratio} variables respectively, for electrons and positrons from $Z \to e^+e^-$ decays with $|\eta_e| < 2.47$ and $E^e_{\mathrm{T}} > 20$ GeV (left plots), or 40 GeV $\leq E^e_{\mathrm{T}} < 50$ GeV (right plots), as simulated at $\sqrt{s} = 8$ TeV with GEANT4 9.4 and 9.6. For the same events and simulation setups, Figure 7 shows the ratio between the energy deposits in the first and second longitudinal layer of the ATLAS LAr EMC. Most of these variables, and especially those associated to the lateral width of the electromagnetic shower, are sensitive to pileup. In order to highlight the impact of the different GEANT4 simulation setups, no pileup overlay is simulated in these samples.

Mild differences are observed in the behavior of the shower shapes when using GEANT4 v. 9.6, with its improved model of the electron multiple scattering, with respect to GEANT4 v. 9.4. Unfortunately, none of these small differences can account for the residual data/MC discrepancies mentioned above [14].

4.2 $Z \to e^+e^-$ line-shape

When comparing data to MC, residual mis-calibration due to calorimeter inhomogeneities or imperfect simulation of passive material are corrected for. The electron and positron transverse energies are corrected in data by a pseudorapidity-dependent scale factor, constrained by comparing the response of the EMC to $Z \to e^+e^-$ events in data and MC [9]. In MC an additional smearing factor is applied to their transverse energies to match the observed energy resolution in data [9]. The $Z \to e^+e^-$ line-shape in data and MC can be compared after the respective corrections have been applied to data and MC, and the residual background contributions in the data sample have been subtracted.

Figure 8 shows the m_{ee} line-shape in pp data at $\sqrt{s} = 8$ TeV compared with the predictions of the $Z \to e^+e^-$ MC samples simulated with GEANT4 9.4 with Urban93 and Urban95, computed for electron and positron candidates impinging the ATLAS LAr EMC at $|\eta_e| < 1$. The corrections described above have been derived separately for the two simulation samples. The bottom pad of Figure 8 shows the corresponding m_{ee} data/MC line-shape ratios. Figures 9 and 10 show similar m_{ee} line-shape comparisons, when restricting the electron and positron pseudorapidity regions to the $|\eta_e| < 0.8$ and $|\eta_e| < 0.6$ regions, respectively.

Before any correction is applied to the simulated samples, the GEANT4 $Z \to e^+e^-$ lineshapes agree to better than 1% in the m_{ee} region between 85 GeVand 95 GeV, while they exibit systematic differences up to 2-3% in the mee tails. When compared to data, after having applied the corrections mentioned above, both GEANT4 versions seem to reproduce the data $Z \to e^+e^-$ lineshape with similar accuracy.

4.3 Fraction of reconstructed photon conversions

Photon candidates are reconstructed in ATLAS from energy deposits in the electromagnetic calorimeter, possibly matched to tracks consistent with a photon conversion in the detector material. Candidate photon conversion vertices get reconstructed from tracks pre-selected as loosely matching electromagnetic energy deposits: they can consist of one or two tracks, where single-track vertices are constructed from tracks that are missing the hit in the innermost layer of the ID despite passing through a functioning detector module. If neither a track nor a vertex is matched to a cluster, the object is considered to be an unconverted photon.

The photon reconstruction procedure has an overall expected efficiency of about 98% for photons with $E_{\mathrm{T}} > 25$ GeV, being on average >99% for unconverted photons, and about 95% for converted photons. The expected fraction of converted photons increases from about 20% at $|\eta_\gamma| \sim 0$ to about 45% at $|\eta_\gamma| \sim 1.6$, due to the increased amount of material in front of the EMC.

In data, photon candidates passing the tight shower-shape based selection, and satisfying the isolation requirement $E_{\mathrm{T}}^{\mathrm{iso}} < 3$ GeV, are expected to have a purity above 80% at $E_{\mathrm{T}}^{\gamma} \sim 25$ GeV, and of better then 99% for $E_{\mathrm{T}}^{\gamma} > 200$ GeV (see for instance Ref. [15]).

Figures 11, 12, 13 and 14 show the fraction of photon candidates reconstructed as converted photons over all selected photon candidates, in the pseudorapidity regions $|\eta_\gamma| < 0.6$, $0.6 \leq |\eta_\gamma| < 1.37$, $1.56 \leq |\eta_\gamma| < 1.81$ and $1.81 \leq |\eta_\gamma| < 2.37$ respectively, for data and MC samples, as a function of the photon candidate energy E^γ. The data are compared with the predictions from `GEANT4` simulations using the `Conv93` and `Conv95` conversion models. For both data and MC, the uncertainties are statistical only. They do not account for any background contamination, nor for possible systematic uncertainties associated with the reconstruction of photon conversions. In general, a qualitatively better agreement between data and MC is observed when the `Conv95` conversion model is used in simulation.

References

[1] ATLAS Collaboration, *The ATLAS Simulation Infrastructure*, The European Physical Journal C **70** (2010) no. 3, 823–874. http://dx.doi.org/10.1140/epjc/s10052-010-1429-9.

[2] S. Frixione, P. Nason, and C. Oleari, *Matching NLO QCD computations with parton shower simulations: the POWHEG method*, JHEP **2007** (2007) no. 11, 070. http://stacks.iop.org/1126-6708/2007/i=11/a=070.

[3] T. Sjöstrand, S. Mrenna, and P. Z. Skands, *A Brief Introduction to PYTHIA 8.1*, Comput. Phys. Commun. **178** (2008) 852–867, arXiv:0710.3820 [hep-ph].

[4] The ATLAS Collaboration, *Charged particle multiplicities in pp interactions for track $p_{\mathrm{T}} > 100$ MeV at $\sqrt{s} = 0.9$ and 7 TeV measured with the ATLAS detector at the LHC*, ATLAS-CONF-2010-046 (2010) . https://cdsweb.cern.ch/record/1281296.

[5] GEANT4 Collaboration, S. Agostinelli et al., GEANT4 - *a simulation toolkit*, Nucl. Instrum. Methods A **506** (2003) 250.

[6] J. Allison, J. Apostolakis, A. Bagulya, C. Champion, S. Elles, F. Garay, V. Grichine, A. Howard, S. Incerti, V. Ivanchenko, J. Jacquemier, M. Maire, A. Mantero, P. Nieminen, L. Pandola, G. Santin, D. Sawkey, A. Schälicke, and L. Urban, *Geant4 electromagnetic physics for high statistic simulation of LHC experiments*, Journal of Physics: Conference Series **396** (2012) no. 2, 022013. http://stacks.iop.org/1742-6596/396/i=2/a=022013.

[7] V.N. Ivanchenko et al., *Geant4 Electromagnetic Physics for LHC Upgrade*, in *Proceedings of CHEP 2013*. 2013. in press.

[8] ATLAS Collaboration, *The ATLAS Experiment at the CERN Large Hadron Collider*, JINST **3** (2008) S08003.

[9] The ATLAS Collaboration, *Electron performance measurements with the ATLAS detector using the 2010 LHC proton-proton collision data*, The European Physical Journal C **72** (2012) no. 3, 1–46. http://dx.doi.org/10.1140/epjc/s10052-012-1909-1.

[10] The ATLAS Collaboration, *Expected photon performance in the ATLAS experiment*, ATL-PHYS-PUB-2011-007 (2011) . https://cds.cern.ch/record/1345329.

[11] M. Cacciari, G. P. Salam, and G. Soyez, *The Catchment Area of Jets*, JHEP **04** (2008) 042.

[12] M. Cacciari, G. P. Salam, and S. Sapeta, *On the characterisation of the underlying event*, JHEP **04** (2010) 065, arXiv:0912.4926 [hep-ph].

[13] The ATLAS Collaboration, *Measurement of the inclusive isolated prompt photon cross section in pp collisions at $\sqrt{s} = 7$ TeV with the ATLAS detector*, Phys.Rev. **D83** (2011) 052005, arXiv:1012.4389 [hep-ex].

[14] The ATLAS Collaboration, *Data/MC Comparison for Calorimeter Shower Shapes of High E_{T} Electrons*, ATLAS Perfomance Plots (2010) . https://atlas.web.cern.ch/Atlas/GROUPS/PHYSICS/EGAMMA/PublicPlots/20111005/ATL-COM-PHYS-2011-1299/index.html.

[15] The ATLAS Collaboration, *Measurement of the inclusive isolated prompt photon cross section in pp collisions at $\sqrt{s} = 7$ TeV with the ATLAS detector using 4.6 fb-1*, arXiv:1311.1440 [hep-ex]. Submitted for publication to Phys. Rev. D.

List of Figures

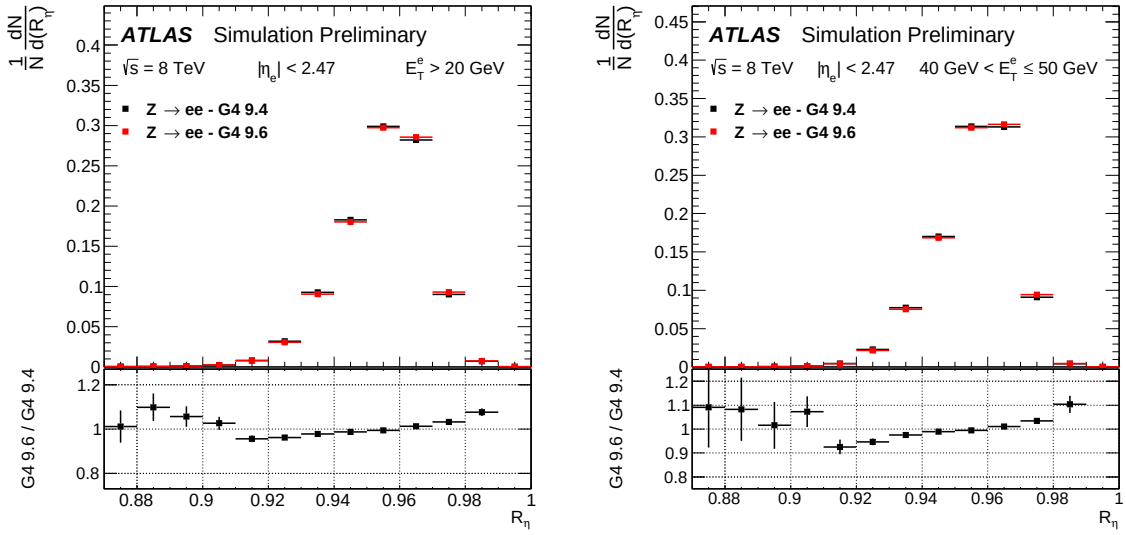

Figure 1: Normalized distribution of R_η for electrons and positrons from $Z \to e^+e^-$ decays, with $|\eta_e| < 2.47$ and $E^e_{\mathrm{T}} > 20$ GeV (left) or 40 GeV $\leq E^e_{\mathrm{T}} < 50$ GeV (right), simulated at $\sqrt{s} = 8$ TeV with GEANT4 9.4 and 9.6. The bottom pads show the ratio between the two GEANT4 simulations.

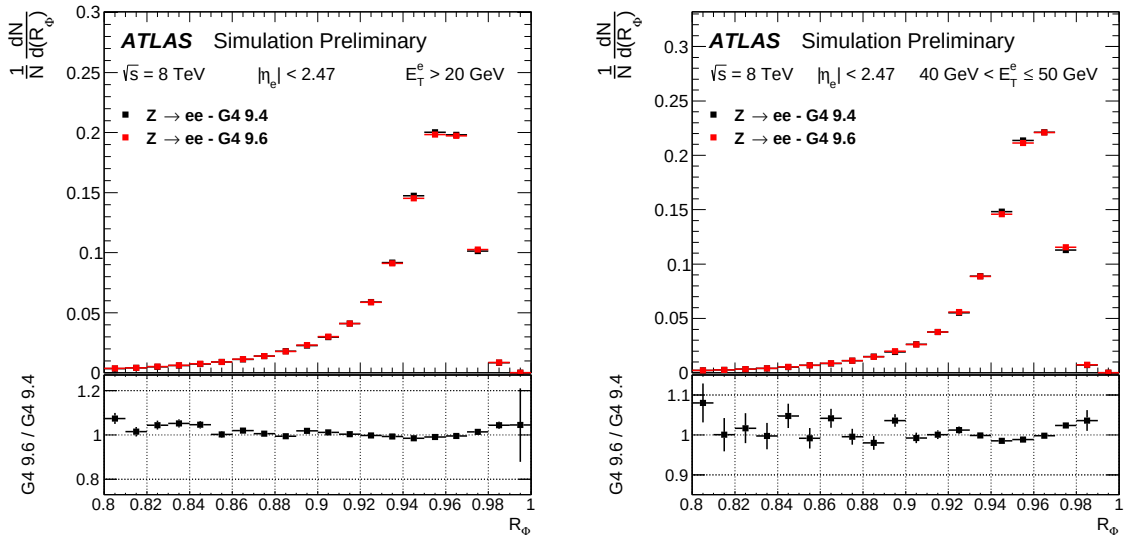

Figure 2: Normalized distribution of R_ϕ for electrons and positrons from $Z \to e^+e^-$ decays, with $|\eta_e| < 2.47$ and $E^e_{\mathrm{T}} > 20$ GeV (left) or 40 GeV $\leq E^e_{\mathrm{T}} < 50$ GeV (right), simulated at $\sqrt{s} = 8$ TeV with GEANT4 9.4 and 9.6. The bottom pads show the ratio between the two GEANT4 simulations.

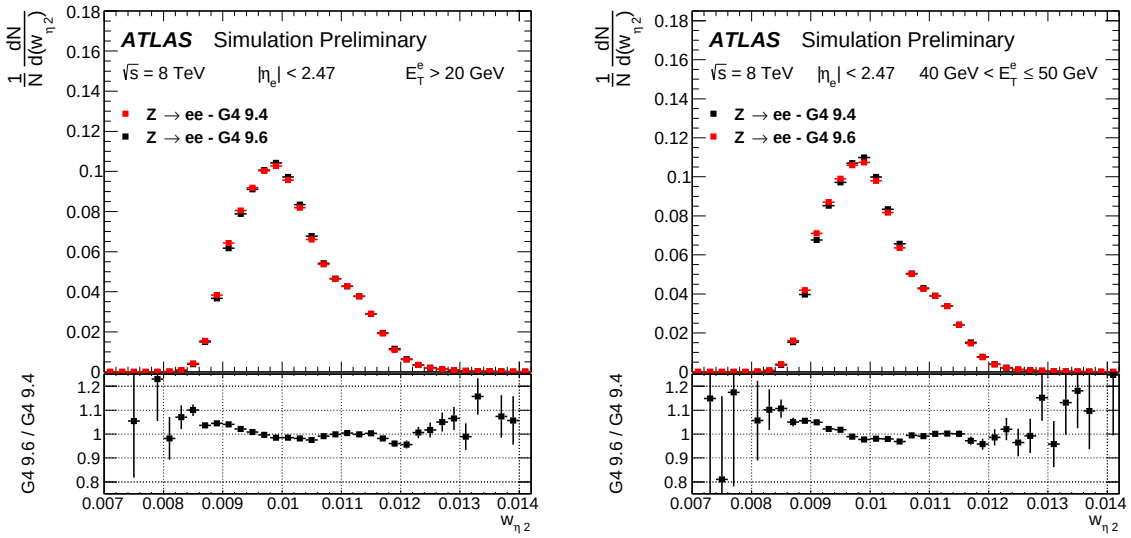

Figure 3: Normalized distribution of w_{η_2} for electrons and positrons from $Z \to e^+e^-$ decays, with $|\eta_e| < 2.47$ and $E^e_{\mathrm{T}} > 20$ GeV (left) or 40 GeV $\leq E^e_{\mathrm{T}} < 50$ GeV (right), simulated at $\sqrt{s} = 8$ TeV with GEANT4 9.4 and 9.6. The bottom pads show the ratio between the two GEANT4 simulations.

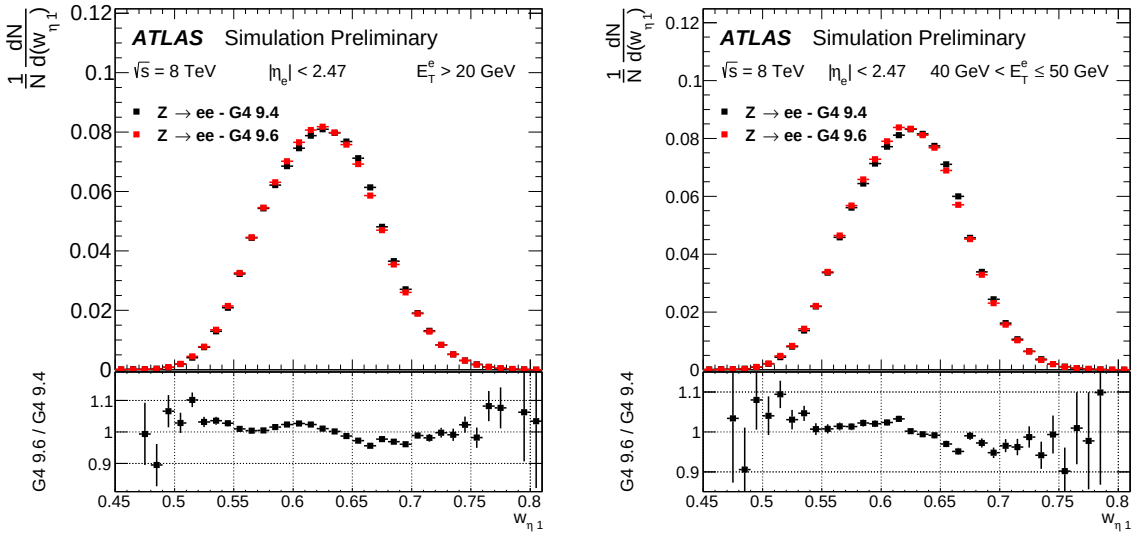

Figure 4: Normalized distribution of $w_{s\,3}$ for electrons and positrons from $Z \to e^+e^-$ decays, with $|\eta_e| < 2.47$ and $E^e_{\mathrm{T}} > 20$ GeV (left) or 40 GeV $\leq E^e_{\mathrm{T}} < 50$ GeV (right), simulated at $\sqrt{s} = 8$ TeV with GEANT4 9.4 and 9.6. The bottom pads show the ratio between the two GEANT4 simulations.

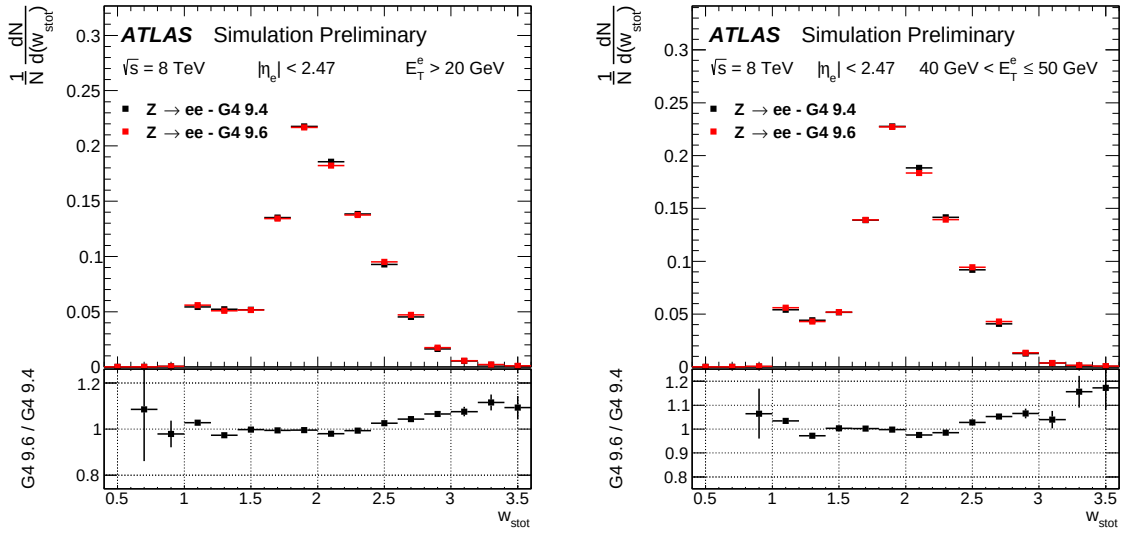

Figure 5: Normalized distribution of $w_{s\,\mathrm{tot}}$ for electrons and positrons from $Z \to e^+e^-$ decays, with $|\eta_e| < 2.47$ and $E^e_{\mathrm{T}} > 20$ GeV (left) or 40 GeV $\leq E^e_{\mathrm{T}} < 50$ GeV (right), simulated at $\sqrt{s} = 8$ TeV with GEANT4 9.4 and 9.6. The bottom pads show the ratio between the two GEANT4 simulations.

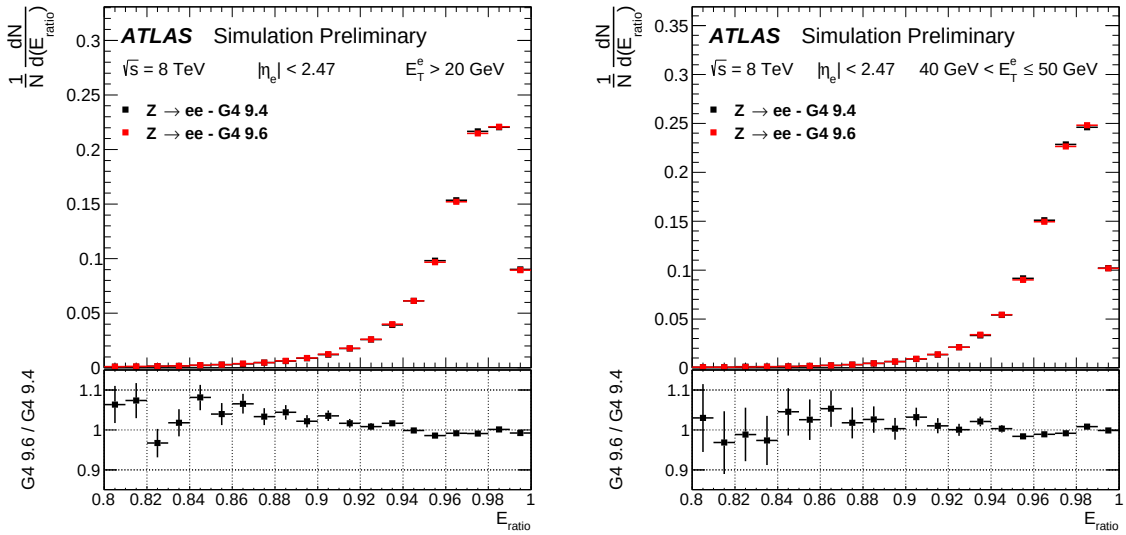

Figure 6: Normalized distribution of E_{ratio} for electrons and positrons from $Z \to e^+e^-$ decays, with $|\eta_e| < 2.47$ and $E^e_{\mathrm{T}} > 20$ GeV (left) or 40 GeV $\leq E^e_{\mathrm{T}} < 50$ GeV (right), simulated at $\sqrt{s} = 8$ TeV with GEANT4 9.4 and 9.6. The bottom pads show the ratio between the two GEANT4 simulations.

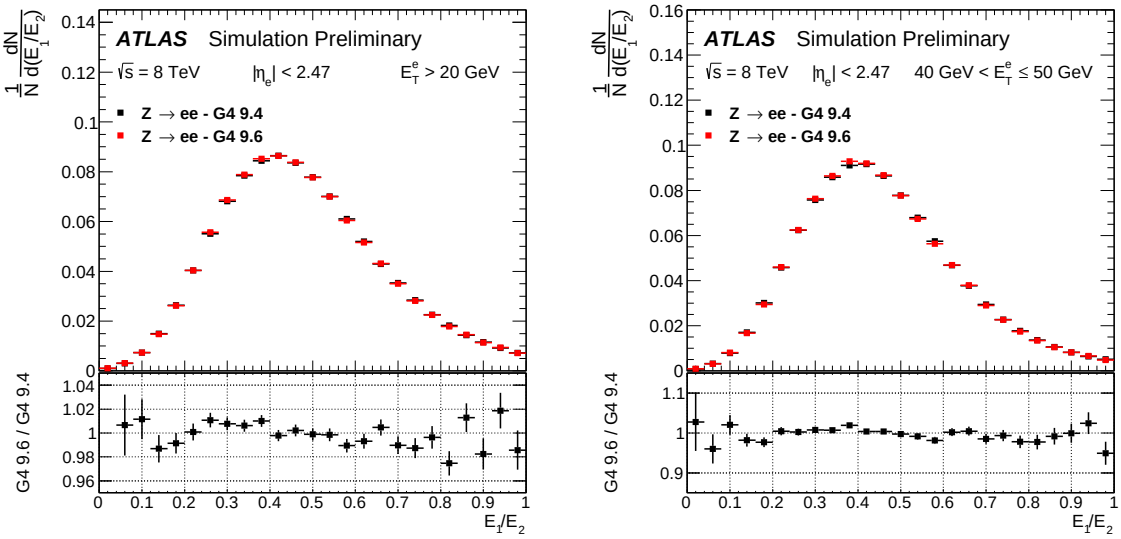

Figure 7: Normalized distribution of E_1/E_2 for electrons and positrons from $Z \to e^+e^-$ decays, with $|\eta_e| < 2.47$ and $E_{\mathrm{T}}^e > 20$ GeV (left) or 40 GeV $\leq E_{\mathrm{T}}^e < 50$ GeV (right), simulated at $\sqrt{s} = 8$ TeV with GEANT4 9.4 and 9.6. The bottom pads show the ratio between the two GEANT4 simulations.

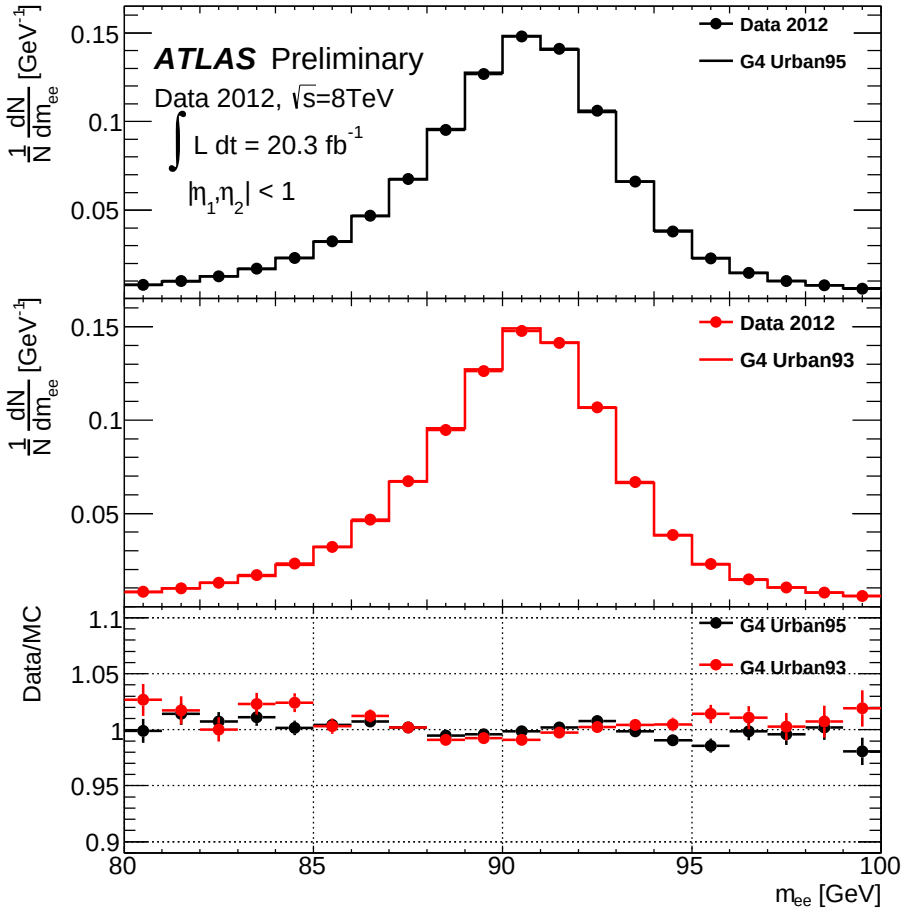

Figure 8: m_{ee} line-shapes in pp data at $\sqrt{s}$ = 8 TeV and for two different $Z \rightarrow e^+e^-$ MC samples simulated with `GEANT4` 9.4 `Urban93` and `Urban95`, computed from electron and positron candidates impinging the ATLAS LAr EMC at $|\eta_e| < 1$. The corrections described in the text have been applied to data and MC respectively, and the residual background components have been subtracted from the data profile. The bottom pad compares the m_{ee} line-shape between data and the alternative MC simulations.

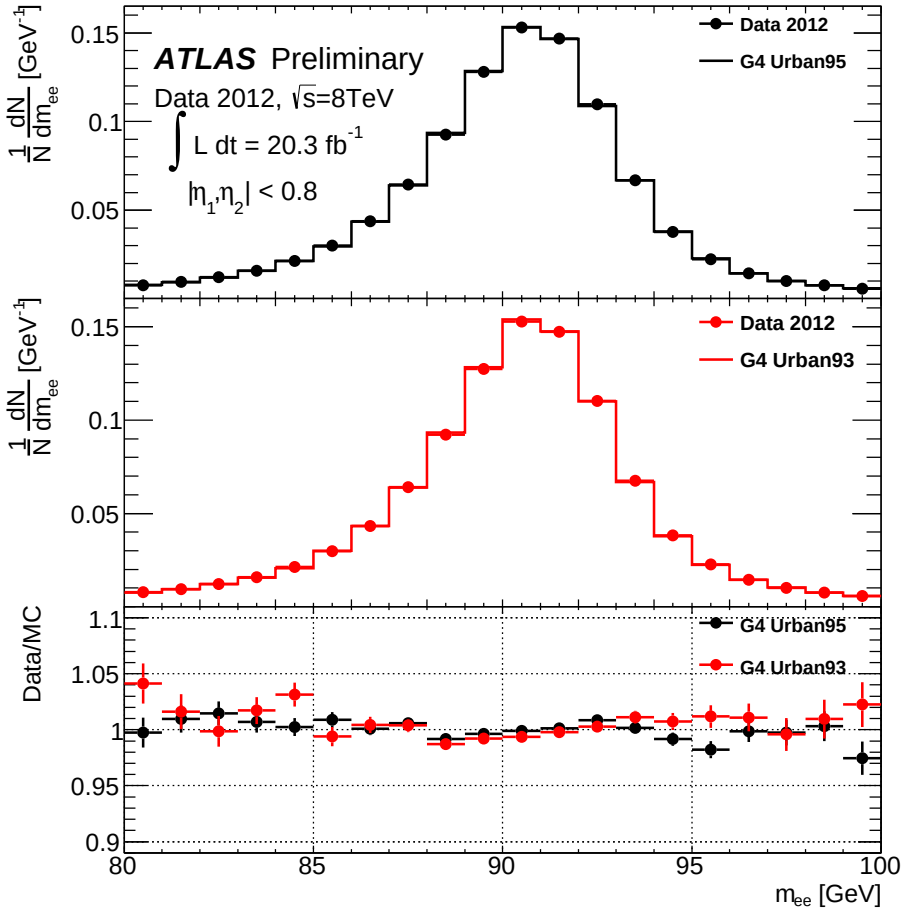

Figure 9: m_{ee} line-shapes in pp data at $\sqrt{s}$ = 8 TeV and for two different $Z \rightarrow e^+e^-$ MC samples simulated with `GEANT4` 9.4 `Urban93` and `Urban95`, computed from electron and positron candidates impinging the ATLAS LAr EMC at $|\eta_e| < 0.8$. The corrections described in the text have been applied to data and MC respectively, and the residual background components have been subtracted from the data profile. The bottom pad compares the m_{ee} line-shape between data and the alternative MC simulations.

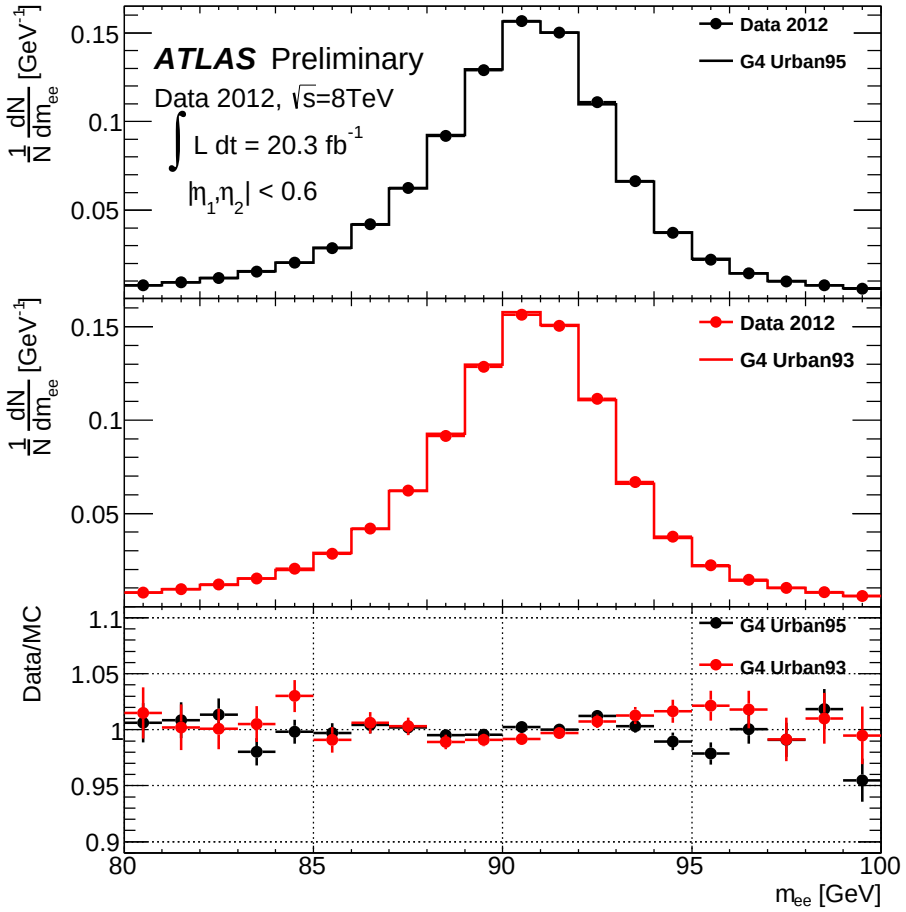

Figure 10: m_{ee} line-shapes in pp data at $\sqrt{s}$ = 8 TeV and for two different $Z \rightarrow e^+e^-$ MC samples simulated with GEANT4 9.4 Urban93 and Urban95, computed from electron and positron candidates impinging the ATLAS LAr EMC at $|\eta_e| < 0.6$. The corrections described in the text have been applied to data and MC respectively, and the residual background components have been subtracted from the data profile. The bottom pad compares the m_{ee} line-shape between data and the alternative MC simulations.

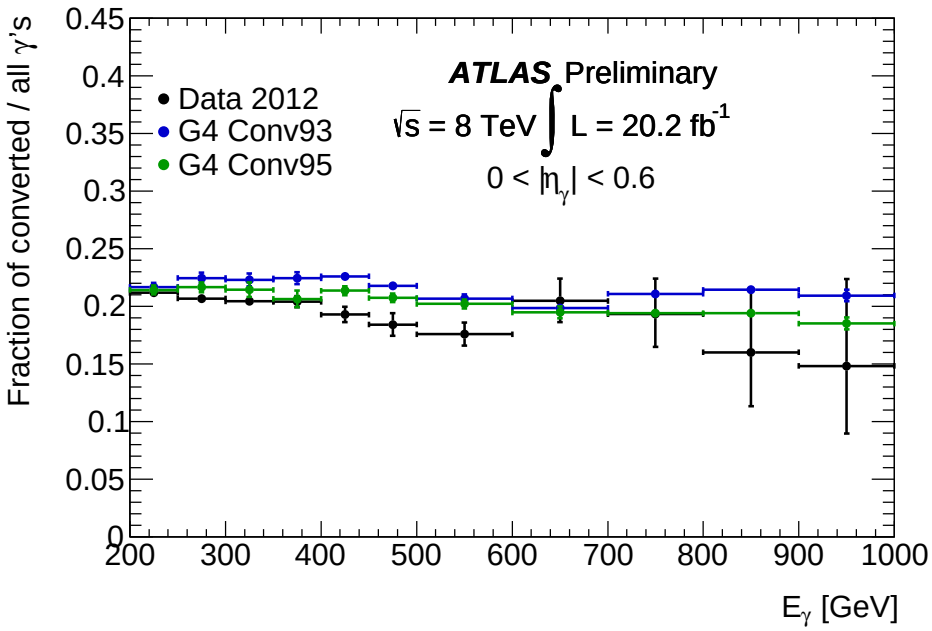

Figure 11: Fraction of photon candidates reconstructed as converted photons over all photons passing the tight quality selection and satisfying the isolation requirement $E_T^{\text{iso}} < 3$ GeV, as function of the reconstructed photon energy E_γ in the pseudorapidity regions $|\eta_\gamma| < 0.6$. The fraction observed in data is compared with those predicted by `GEANT4` simulations using `Conv93` and `Conv95` conversion models. Only statistical uncertainties are displayed.

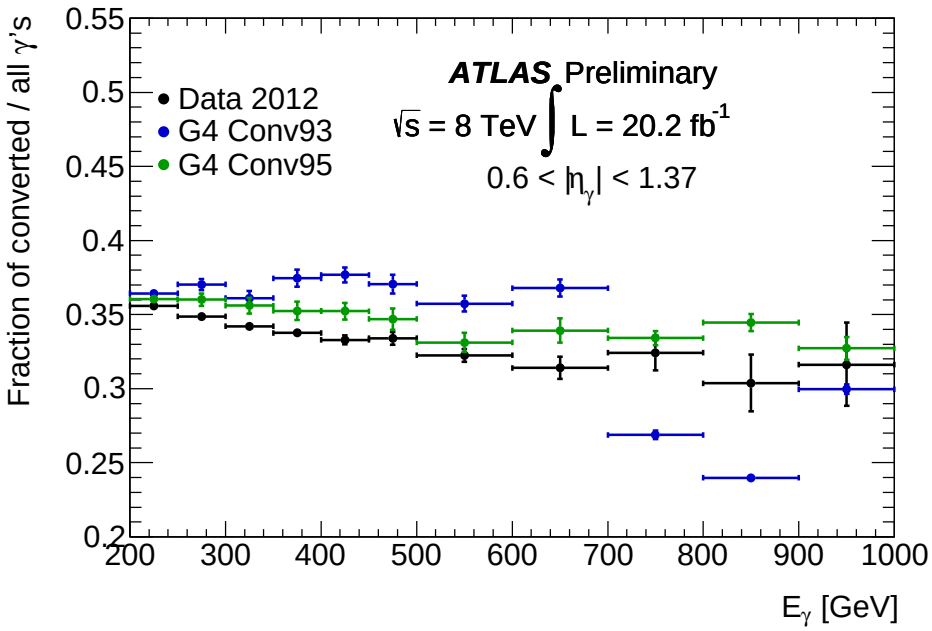

Figure 12: Fraction of photon candiates reconstructed as converted photons over all photons passing the tight quality selection and satisfying the isolation requirement $E_T^{\text{iso}} < 3$ GeV, as function of the reconstructed photon energy E_γ in the pseudorapidity regions $0.6 \leq |\eta_\gamma| < 1.37$. The fraction observed in data is compared with those predicted by `GEANT4` simulations using `Conv93` and `Conv95` conversion models. Only statistical uncertainties are displayed.

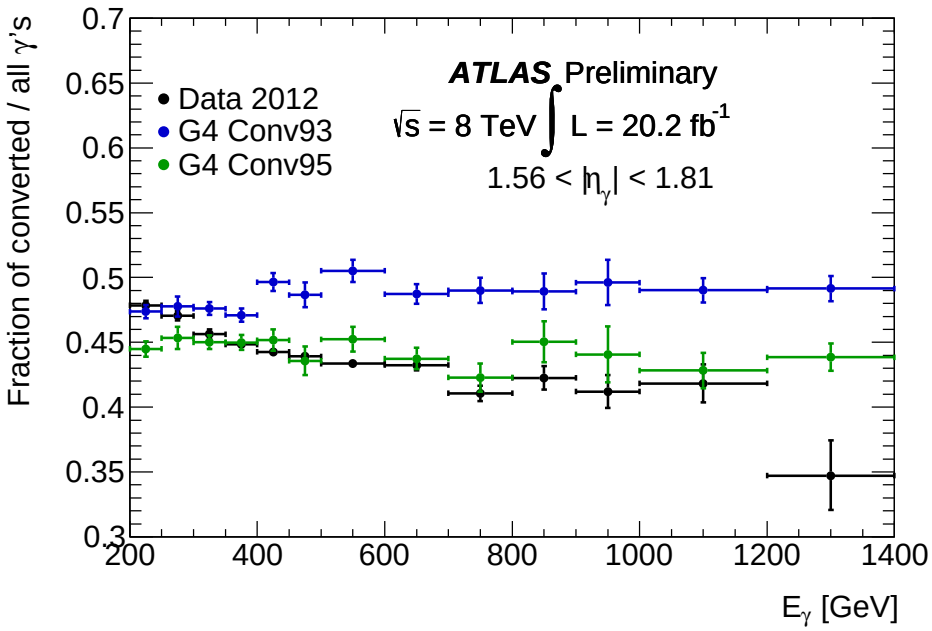

Figure 13: Fraction of photon candidates reconstructed as converted photons over all photons passing the tight quality selection and satisfying the isolation requirement $E_T^{\text{iso}} < 3$ GeV, as function of the reconstructed photon energy E_γ in the pseudorapidity regions $1.56 \leq |\eta_\gamma| < 1.81$. The fraction observed in data is compared with those predicted by `GEANT4` simulations using `Conv93` and `Conv95` conversion models. Only statistical uncertainties are displayed.

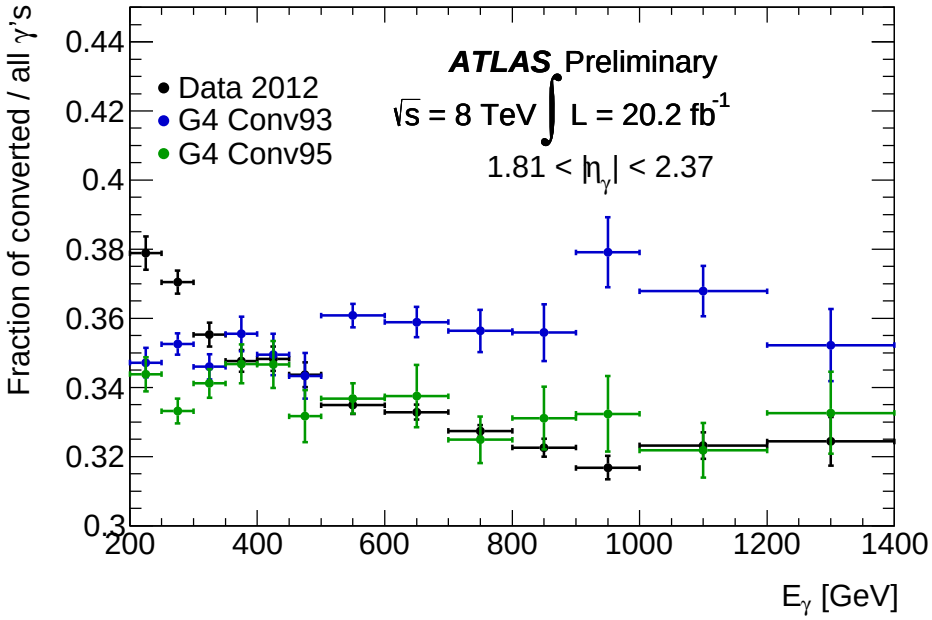

Figure 14: Fraction of photon candidates reconstructed as converted photons over all photons passing the tight quality selection and satisfying the isolation requirement $E_T^{\text{iso}} < 3$ GeV, as function of the reconstructed photon energy E_γ in the pseudorapidity regions $1.81 \leq |\eta_\gamma| < 2.37$. The fraction observed in data is compared with those predicted by `GEANT4` simulations using `Conv93` and `Conv95` conversion models. Only statistical uncertainties are displayed.